

Ground and excited state properties of pyrene, azapyrene, diazapyrene and derivatives

Master Internship Report

Yuan-Wei Pi



Freie Universität Berlin

Supervisor

Prof. Dr. Beate Paulus

M.Sc. Felix Witte

Abbreviations

ACN	acetonitrile
def2-TZVP	Ahlrichs' Turbomole default valence polarized triple-zeta basis set
BP86	Becke (B) and Perdew (P86) exchange correlation functional
B3-LYP	Becke 3-parameter Lee-Yang-Parr hybrid functional
BH-LYP	Becke half-and-half Lee-Yang-Parr hybrid functional
COSMO	conductor-like screening model
DFT	density functional theory
DCM	dichloromethane
XC	exchange-correlation
GGA	generalized gradient approximation
D3(BJ)	Grimme's D3 dispersion correction and Becke-Johnson damping
HF	Hartree-Fock
HOMO	highest occupied molecular orbital
HK	Hohenberg-Kohn
LDA	local density approximation
LUMO	lowest unoccupied molecular orbital
mGGA	meta-GGA
M06-2X	Minnesota (2006) hybrid mGGA functional with 54 % HF exchange
PBE0	Perdew-Burke-Ernzerhof hybrid functional
PES	potential energy surface
SCF	self-consistent field (method)
TDDFT	time-dependent DFT

Contents

Abbreviations	i
List of Figures	iii
List of Tables	iv
1 Introduction	1
2 Theoretical foundations	2
2.1 Density Functional Theory	2
2.2 Time-dependent Density Functional Theory	8
2.3 Solvent models	10
2.4 Franck–Condon principle	10
3 Computational details	12
3.1 Molucules in the calculations	12
3.2 Calculation Procedure	12
3.3 Conductor like Screening Model (COSMO)	14
4 Results and Discussion	15
4.1 Comparison of relative energies	15
4.2 Acetonitrile (ACN) vs.Dichloromethane (DCM) solvent	16
4.3 Comparison of different DFT functionals	17
4.4 Comparison of calculations and experiments	18
4.5 Analysis of electronic transition	20
5 Summary and Outlook	27
Bibliography	28

List of Figures

2.1	Franck Condon diagram	11
3.1	Molecules in the calculations	12
3.2	Calculation workflow	13
4.1	Relative energies of azapyrene derivatives	15
4.2	Relative energies of diazapyrene derivatives	16
4.3	Pyrene HOMO/LUMO gap with different functionals with def2-TZVP basis set	17
4.4	2,7-diazapyrene HOMO/LUMO gap with different functionals with def2-TZVP basis set	18
4.5	DCM pyrene spectrum	19
4.6	ACN 2,7-diazapyrene spectrum	19
4.7	Pyrene orbitals, ground and excited state bond length	21
4.8	1-azapyrene orbitals, ground and excited state bond length	22
4.9	2-azapyrene orbitals, ground and excited state bond length	23
4.10	4-azapyrene orbitals, ground and excited state bond length	24
4.11	2,7-diazapyrene orbitals, ground and excited state bond length	25
4.12	2,10-diazapyrene orbitals, ground and excited state bond length	26

List of Tables

4.1	HOMO/LUMO gap of different solvents	16
4.2	HOMO/LUMO gap of different functionals with def2-TZVP basis set . . .	17

1 Introduction

Pyrene is an apolar and highly symmetrical polycyclic aromatic compound, composed of four fused benzene rings [5]. Its structural features lead to a sensitive property of spectrum to the polarity of its environment [8]. Thus, it is useful as a molecular spectroscopic probe in the research of biomolecules. Its spectral feature can be used to obtain information such as protein structure, molecular organization and conformation [9].

On the other hand, the solvent and its concentration influence the fluorescence intensity [23]. The solvent molecules are responsible for the change in molecular geometry, electronic structure and dipolar moment of the solute [18]. Therefore, they cause solvatochromic shifts in absorption and emission spectra [10].

Also, nitrogen attracts surrounding electrons due to its high electrogravity. Thus, the nitrogen substitution on pyrene has a strong influence on the electronic structure. On different positions, nitrogen substitution has a different effect. Moreover, the number of nitrogen substitutions is a factor as well. Hence, our calculations include azapyrene (one-nitrogen substitution) and dizapyrene (two-nitrogen substitution) with their isomers to study these effects.

Aforementioned, the motivation comes from the different fluorescence properties of the pyrene and its derivatives. These characteristics lead to further application as a probe in spectroscopy. Therefore, the goal of this report is to focus on pyrene's properties and find out the influence of nitrogen substitution on different positions. In order to obtain spectral information, analysis of the ground state and excited state properties are performed. Moreover, due to solvent effects on the fluorescence, different solvents are considered in the calculations as well.

2 Theoretical foundations

2.1 Density Functional Theory

Thomas and Fermi lay the foundations for density functional theory (DFT), formulating electronic many-body system in terms of electron density [25]. With this concept, for an N -electron system, it can be described by 3 dimensional quantum mechanics system in the calculation.

2.1.1 Hohenberg and Kohn theorems

Later, Hohenberg and Kohn elaborated this concept by dealing with the non-degenerated ground state of an interacting electron gas in an external potential $v(\mathbf{r})$ as the Hohenberg and Kohn theorems (HK theorems) [11]. The first HK theorem pointed out that the external potential is a unique functional of the electron density. The proof proceeds by *reductio ab absurdum*. The Hamiltonian operator in this case is defined as the sum of kinetic operator of the N -particles system, electron-electron Coulomb interaction and external potential,

$$\hat{H} = \hat{T} + \hat{V} + \hat{U} \quad (2.1)$$

where

$$\hat{T} = - \sum_{i=1}^N \frac{1}{2} \nabla_i \quad (2.2)$$

$$\hat{V} = \sum_{i=1}^N v(\mathbf{r}_i) \quad (2.3)$$

$$\hat{U} = \sum_{i=1}^N \sum_{i < j}^N \frac{1}{r_{ij}} \quad (2.4)$$

with the ground state ψ . Assume another system with $v'(\mathbf{r})$ and the ground state ψ' ($\psi \neq \psi'$) results in the same density $\rho(\mathbf{r})$ (unless the case of $v'(\mathbf{r}) - v(\mathbf{r}) = const$). And these two systems satisfy different Time-independent Schrödinger equations,

$$\hat{H}\psi = E\psi \quad (2.5)$$

$$\hat{H}'\psi' = E'\psi' \quad (2.6)$$

2.1 Density Functional Theory

where the Hamiltonian and ground state energies associated with ψ and ψ' are H', H and E, E' , respectively. According to the vibrational principle, we can write,

$$E' = \langle \psi' | H' | \psi' \rangle < \langle \psi | H' | \psi \rangle = \langle \psi | H + \hat{V}' - \hat{V} | \psi \rangle \quad (2.7)$$

$$E' < \langle \psi | H' | \psi \rangle + \langle \psi | \hat{V}' - \hat{V} | \psi \rangle = E + \int [v'(\mathbf{r}) - v(\mathbf{r})] \rho(\mathbf{r}) d\mathbf{r} \quad (2.8)$$

Interchanging the primed in Eq. 2.8 in the same way and obtain

$$E < E' + \int [v'(\mathbf{r}) - v(\mathbf{r})] \rho(\mathbf{r}) d\mathbf{r} \quad (2.9)$$

The addition of Eq. 2.8 and Eq. 2.9 shows

$$E + E' < E + E', \quad (2.10)$$

which contradicts the initial assumption. Thus $v(\mathbf{r})$ is a unique functional of $\rho(\mathbf{r})$.

The HK second theorem states that if and only if the density is the true ground state density, the functional that describe the ground state energy results in the lowest energy. To prove the theorem, we define a universal functional $F[\rho(\mathbf{r})]$, which is valid for any number of particles and external potential

$$F[\rho(\mathbf{r})] \equiv \langle \psi | \hat{T} + \hat{U} | \psi \rangle \quad (2.11)$$

and redefine the functional for the energy $E_v[\rho(\mathbf{r})]$

$$E_v[\rho(\mathbf{r})] = \langle \psi | \hat{H} | \psi \rangle = F[\rho(\mathbf{r})] + \int v(\mathbf{r}) \rho(\mathbf{r}) d\mathbf{r} \quad (2.12)$$

Obviously, with the true ground state density, $E_v[\rho(\mathbf{r})]$ is equal to ground state energy. And $\rho(\mathbf{r})$ has the condition

$$N[\rho] \equiv \int \rho(\mathbf{r}) d\mathbf{r} = N \quad (2.13)$$

Therefore, we can write the energy functional of ψ' for a system of N particles as

$$E_v[\psi'] = \langle \psi' | \hat{V} | \psi' \rangle + \langle \psi' | \hat{T} + \hat{U} | \psi' \rangle \quad (2.14)$$

which has a minimum at the correct ground state ψ . Then let ψ' be the ground state associated with a different external potential $v'(\mathbf{r})$. Combine Eq. 2.10 and Eq. 2.13,

$$E_v[\psi'] = \int v(\mathbf{r}) \rho'(\mathbf{r}) d\mathbf{r} + F[\rho'(\mathbf{r})] \quad (2.15)$$

$$\geq E_v[\psi] = \int v(\mathbf{r}) \rho(\mathbf{r}) d\mathbf{r} + F[\rho(\mathbf{r})] \quad (2.16)$$

The equality holds if and only if $\psi' = \psi$. That is to say, the density that minimizes the total energy is the exact ground state density.

In sum, the HK theorem showed that there exists a one-to-one mapping between v -representable electronic densities and external potentials. A v -representable density is a ground state density that can be associated with a Hamiltonian that has an external

2 Theoretical foundations

potential. However, the HK theorem is not valid for non-degenerate ground states [16]. To solve this problem, Levy-Leib Constrained-search formulation reformed the HK variational problem and defined the exact HK functional to be N -representable.

2.1.2 Levy-Leib Constrained-search Formulation

The formulation extended minimization algorithm required the densities only N -representable [15]. Here, the condition of v -representable was removed and variational problem requires only antisymmetric wavefunction and the intergration over densities is equal to the number of particles in the system

$$N[\rho] \equiv \int \rho(\mathbf{r}) d\mathbf{r}. \quad (2.17)$$

Rewrite the variational problem in the HK theorem as,

$$\langle \psi_{\rho_0} | \hat{H} | \psi_{\rho_0} \rangle \geq \langle \psi_0 | \hat{H} | \psi_0 \rangle = E_0 \quad (2.18)$$

$$\langle \psi_{\rho_0} | \hat{T} + \hat{U} | \psi_{\rho_0} \rangle + \int v(\mathbf{r}) \rho_0(\mathbf{r}) d\mathbf{r} \geq \langle \psi_0 | \hat{T} + \hat{U} | \psi_0 \rangle + \int v(\mathbf{r}) \rho_0(\mathbf{r}) d\mathbf{r} \quad (2.19)$$

where ψ_{ρ_0} is not the ground state of \hat{H} . We can simply cancel out the external potential term on both side

$$\langle \psi_{\rho_0} | \hat{T} + \hat{U} | \psi_{\rho_0} \rangle \geq \langle \psi_0 | \hat{T} + \hat{U} | \psi_0 \rangle \quad (2.20)$$

which removes the v -representable condition. Among the wavefunctions giving the same ρ_0 , the ground state wavefunction ψ_0 minimizes the quantity $\langle \psi_{\rho_0} | \hat{T} + \hat{U} | \psi_{\rho_0} \rangle$. That is, the minimization of the unirversal functional,

$$F[\rho] = \min_{\psi \rightarrow \rho} \langle \hat{T} + \hat{U} | \psi | \hat{T} + \hat{U} \rangle \quad (2.21)$$

is searching over all antisymmetric wavefunction that yield ρ_0 , then $F[\rho_0]$ delivers the minimum of $\langle \psi_{\rho_0} | \hat{T} + \hat{U} | \psi_{\rho_0} \rangle$. From the point of view of total energy, we obtain the reformation of the variational problem,

$$E_0 = \min_{\psi} \langle \psi | \hat{H} | \psi \rangle \quad (2.22)$$

Then with Eq. 2.20, we obtain

$$E_0 = \min_{\rho} \left[\min_{\psi \rightarrow \rho} \left(\langle \psi | \hat{T} + \hat{U} | \psi \rangle + \int v(\mathbf{r}) \rho(\mathbf{r}) d\mathbf{r} \right) \right] \quad (2.23)$$

where the inner minimization is restricted to all wavefunctions leading to $\rho(\mathbf{r})$; the outer minimization searches over all the ρ which integrate to N . This showed the point of view of computation in searching the required energy. And the only condition is that the integration over densities must equal to the number of particles in the system.

2.1.3 Kohn-Sham method

To compute the information of the ground state, Kohn and Sham developed a method to write the exact ground state density as the ground state density of a fictitious system of non-interacting particles. This provided self-consistent equations that can be numerically solved [26].

To begin with, we write the energy of the interacting system as

$$E[\rho] = \int \rho(\mathbf{r})v(\mathbf{r})d\mathbf{r} + F[\rho] \quad (2.24)$$

where $F[\rho] = T[\rho] + U[\rho]$. The minimization of Eq. 2.24 leads to the ground state density. Thus, by minimizing it we can get the Euler equation,

$$\delta_\rho[E[\rho] - \mu \int \rho(\mathbf{r})d\mathbf{r}] = 0 \quad (2.25)$$

$$\mu = v(\mathbf{r}) + \frac{\delta F[\rho]}{\delta \rho} \quad (2.26)$$

where μ is a Langrange multiplier associated with the constraint described $\int \rho(\mathbf{r})d\mathbf{r} = N$.

In the system, we only know part of $U[\rho]$ analytically, and do not generally know about $T[\rho]$. Therefore, Kohn and Sham introduced a exchange-correlation term $E_{xc}[\rho]$ which is the analytically unknown part in $U[\rho]$

$$U[\rho] = \frac{1}{2} \int \int \frac{\rho(\mathbf{r})\rho(\mathbf{r}')}{|\mathbf{r} - \mathbf{r}'|} d\mathbf{r} d\mathbf{r}' \quad (2.27)$$

$$= J[\rho] + E_{xc}[\rho] \quad (2.28)$$

and introduced Kohn-Sham orbitals φ_i , which is a orbital of single particle. The system with ψ_i for each electron corresponds to implicit physical assumption of non-interacting electrons. Thus, they rewrote the Hamiltonian of non-interacting electrons as

$$\hat{H}_{non-int} = \sum_{i=1}^N -\frac{1}{2} \nabla_i^2 + \sum_{i=1}^N v_{non-int}(r_i), \quad (2.29)$$

with the density

$$\rho(\mathbf{r}) = \int_{i=1}^N |\varphi_i(\mathbf{r})| \quad (2.30)$$

and for single particle and with the aim of Slater determinant, the one-electron Schrödinger equation can be written as

$$\hat{h}_{non-int}\varphi_i = [-\frac{1}{2} \nabla_i^2 + v_{non-int}(r_i)]\varphi_i \quad (2.31)$$

$$= \epsilon_i \varphi_i \quad (2.32)$$

So we can obtain the energy of the non-interacting system with

$$E_{non-int}[\rho] = T_{non-int}[\rho] + v[\rho] \quad (2.33)$$

2 Theoretical foundations

and the universal functional of interacting system can be written as

$$F[\rho] = T[\rho] - T_{non-int}[\rho] + U[\rho] - J[\rho] \quad (2.34)$$

$$= T_{non-int}[\rho] + E_{XC}[\rho] + J[\rho] \quad (2.35)$$

Then go back to the Lagrange multiplier μ in Eq. 2.26 and the Euler equation , we can rewrite μ as

$$\mu = v_{eff}(\mathbf{r}) + \frac{\delta T_{non-int}[\rho]}{\delta \rho}, \quad (2.36)$$

and the effective potential v_{eff} is the sum of external potential $v(\mathbf{r})$, Coulomb interaction $v_J(\mathbf{r})$ and exchange-correlation potential $v_{xc}(\mathbf{r})$.

$$v_{eff}(\mathbf{r}) = v(\mathbf{r}) + \frac{\delta J[\rho]}{\delta \rho(\mathbf{r})} + \frac{\delta E_{xc}[\rho]}{\delta \rho(\mathbf{r})} \quad (2.37)$$

$$= v(\mathbf{r}) + \int \frac{\rho(\mathbf{r}')}{|\mathbf{r} - \mathbf{r}'|} + v_{xc}(\mathbf{r}) \quad (2.38)$$

$$= v(\mathbf{r}) + v_J(\mathbf{r}) + v_{xc}(\mathbf{r}) \quad (2.39)$$

In practice, the ground state problem can be solved self-consistently. First, begin with a ground state $\rho_i(\mathbf{r})$, then construct effective potential v_{eff} in Eq. 2.37. Second, solve for φ_i and gives a new $\rho_{i+1}(\mathbf{r})$ from Eq. 2.30. Last, we repeat the first and second step until the energy is converged.

2.1.4 Functionals approximations

The only unknown part in the Kohn and Sham density functional theory is the exchange-correlation energy. In the past decades, several functionals have been developed. For example, the local density approximation (LDA), in which the electron density is viewed as a uniform density in the system [21]. The LDA exchange-correlation energy is written as

$$E_{xc}^{LDA}[\rho] = \int \rho(\mathbf{r}) \varepsilon_{XC}(\rho(\mathbf{r})) d\mathbf{r} \quad (2.40)$$

where ρ is the electronic density and ε_{XC} is the exchange-correlation energy per particle of a homogeneous electron gas.

Further, if we considered the changes in density, an inhomogeneous system, which means the density is not uniform, the generalized gradient approximation (GGA) is established [13]. The GGA exchange-correlation energy is written as an integral over a function f consisting of the density and its first derivative

$$E_{xc}^{GGA}[\rho] = \int f(\rho(\mathbf{r}), \nabla \rho(\mathbf{r})) d\mathbf{r} \quad (2.41)$$

Moreover, the extension of GGA is meta-GGA (mGGA). It contains the Laplacian (second derivative) of the density to achieve higher accuracy. However in practice, it includes the non-interacting kinetic energy density $\tau(\mathbf{r})$ instead of the Laplacian because it is numerically

2.1 Density Functional Theory

more stable [2]. Thus, the meta-GGA energy is written as an integral over a function g consisting of the density and its first derivative, as well as the energy density $\tau(\mathbf{r})$

$$E_{xc}^{\text{Meta-GGA}}[\rho] = \int g(\rho(\mathbf{r}), \nabla\rho(\mathbf{r}), \tau(\mathbf{r})) d\mathbf{r} \quad (2.42)$$

where the non-interacting kinetic energy density $\tau(\mathbf{r})$ is defined as

$$\tau(\mathbf{r}) = \frac{1}{2} \sum_{i=1}^N |\nabla\psi_i(\mathbf{r})| \quad (2.43)$$

The exchange-correlation energy can be decomposed as the linear sum of exchange and correlation term

$$E_{xc} = E_x + E_c \quad (2.44)$$

Therefore, functionals can be separated into exchange and correlation contribution. Hybrid functionals, which were applied in this project, make a bigger difference in cost and accuracy. It is a linear combination of exact exchange from Hartree–Fock theory and the exchange-correlation energy [1]. The Hartree–Fock exact exchange is

$$E_x^{\text{HF}} = -\frac{1}{2} \sum_{i,j} \int \int \frac{\psi_i^*(\mathbf{r})\psi_j^*(\mathbf{r}')\psi_i(\mathbf{r})\psi_j(\mathbf{r}')}{|\mathbf{r} - \mathbf{r}'|} d\mathbf{r} d\mathbf{r}' \quad (2.45)$$

The coefficient of in the linear combination determines the weight of the individual functional based on the different case. Take B3-LYP (Becke, 3-parameter, Lee–Yang–Parr) exchange-correlation functional [14] as an example, it is defined as

$$E_{xc}^{\text{B3-LYP}} = E_x^{\text{LDA}} + a_0(E_x^{\text{HF}} - E_x^{\text{LDA}}) + a_x(E_x^{\text{GGA}} - E_x^{\text{LDA}}) \quad (2.46)$$

$$+ E_c^{\text{LDA}} + a_c(E_c^{\text{GGA}} - E_c^{\text{LDA}}) \quad (2.47)$$

$$E_x^{\text{LDA}} = E_x^{\text{VWN}}; E_x^{\text{GGA}} = E_x^{\text{B88}}; E_c^{\text{GGA}} = E_c^{\text{B88}}$$

where $a_0, a_x = 0.72$, and $a_c = 0.81$.

2.1.5 Functionals in the project

Besides B3-LYP, which is mentioned in previous section and used in this project, this project also includes Becke-Half-and-Half-LYP functional (BH-LYP) [20], Perdew–Burke–Ernzerhof hybrid functional (PBE0) [12] and Minnesota (2006) hybrid mGGA functional with 54 % HF exchange (M06-2X) [27]. Below are their definition.

BH-LYP is defined as 1:1 mixture of DFT and exact exchange energies,

$$E_{xc}^{\text{BH-LYP}} = \frac{1}{2} E_x^{\text{HF}} + \frac{1}{2} E_x^{\text{B88}} + E_c^{\text{LYP}} \quad (2.48)$$

PBE0 mixes the Perdew–Burke–Ernzerhof (PBE) exchange energy and Hartree-Fock

2 Theoretical foundations

exchange energy, and PBE exchange-correlation energy is

$$E_{xc}^{PBE} = \frac{1}{4}E_x^{HF} + \frac{3}{4}E_x^{PBE} + E_c^{PBE}, \quad (2.49)$$

M06-2X is one of the Minnesota functional, a meta hybrid GGA. It is parametersized with focus on dispersive interactions.

Due to the lack of van-der-Waals (dispersive) interactions in long range, B3-LYP, BH-LYP, PBE0 DFT calculations involve Grimme's D3 dispersion correction and Becke-Johnson damping method (D3-(BJ)) [24] for the correction.

2.2 Time-dependent Density Functional Theory

The time-dependent density functional theory (TD-DFT) extends DFT to time dependent Hamiltonians,

$$\hat{H}(\mathbf{r}, t) = \hat{T}(\mathbf{r}) + \hat{V}_{ext}(\mathbf{r}, t) + \hat{U}(\mathbf{r}) \quad (2.50)$$

Here, we deal with the time-dependent Schrödinger equation

$$i\frac{\partial}{\partial t}\Psi(\mathbf{r}, t) = \hat{H}(\mathbf{r}, t)\Psi(\mathbf{r}, t). \quad (2.51)$$

2.2.1 Runge-Gross theorem

In the Runge-Gross theorem[22], there exists a one-to-one mapping between the external time-dependent potential and the time-dependent electronic one-body density. This can be proved by the continuity equation with *reductio ad absurdum*, which is analogous to the HK theorem.

First, assume that the difference of two potential is more than an additive spatially independent term, and are expendable in a Taylor series, which means

$$u_k(\mathbf{r}) \equiv \frac{\partial^k}{\partial t^k}(v(\mathbf{r}, t) - v'(\mathbf{r}, t))\Big|_{t=t_0}, \quad k \geq 0 \quad (2.52)$$

is not a constant in space. And the continuity equation derived from Gauss's law in the differential form indicates the relation between electronic density ρ and current density \mathbf{j} ,

$$\frac{\partial \rho(\mathbf{r}, t)}{\partial t} + \nabla \cdot \mathbf{j}(\mathbf{r}, t) = 0 \quad (2.53)$$

Now assume two different densities ρ and ρ' , and current densities \mathbf{j} and \mathbf{j}' , and apply them to the previous assumption,

$$\frac{\partial^{k+2}}{\partial t^{k+2}}(\rho(\mathbf{r}, t) - \rho'(\mathbf{r}, t))\Big|_{t=t_0} = -\nabla \cdot \frac{\partial^{k+1}}{\partial t^{k+1}}(j(\mathbf{r}, t) - j'(\mathbf{r}, t))\Big|_{t=t_0} \quad (2.54)$$

$$= -\nabla \cdot \left[\frac{\rho(\mathbf{r}, t_0)\partial^k}{\partial t^k}(v(\mathbf{r}, t_0) - v'(\mathbf{r}, t_0))\Big|_{t=t_0} \right] \quad (2.55)$$

$$= -\nabla \cdot [\rho(\mathbf{r}, t_0)\nabla u_k(\mathbf{r})]. \quad (2.56)$$

This indicates that the two densities will be different if the right-hand-side is non-zero.

Then assume that the right-hand-side is zero on the contrary,

$$\nabla \cdot (\rho(\mathbf{r}, t_0) \nabla u_k(\mathbf{r})) = 0. \quad (2.57)$$

and integrate over all space with Green's theorem,

$$0 = \int d\mathbf{r} u_k(\mathbf{r}) \nabla \cdot (\rho(\mathbf{r}, t_0) \nabla u_k(\mathbf{r})) \quad (2.58)$$

$$= - \int d\mathbf{r} \rho(\mathbf{r}, t_0) (\nabla u_k(\mathbf{r}))^2 + \frac{1}{2} \int d\mathbf{S} \cdot \rho(\mathbf{r}, t_0) (\nabla u_k^2(\mathbf{r})). \quad (2.59)$$

In finite systems, the density decays to zero exponentially. And $\nabla u_k^2(\mathbf{r})$ increases slower than the density decays. Thus, the surface integral vanishes. Due to the non-negativity of the density,

$$\rho(\mathbf{r}, t_0) (\nabla u_k(\mathbf{r}))^2 = 0, \quad (2.60)$$

where u_k is a constant. This shows the contradiction between the original assumption and the proof. The proof points out that the electronic density changes in response to the external potential, such as a time-varying electric field.

2.2.2 Time-dependent Kohn-Sham system

The Runge-Gross theorem shows that the time-dependent external potential uniquely determines the time-dependent density. Thus, the Kohn-Sham method is applicable for time-dependent cases [17]. Again we can write the time-dependent Schrödinger equation with time-dependent Kohn-Sham effective potential v_{eff} and Kohn-Sham orbitals φ_i

$$i \frac{\partial}{\partial t} \varphi_i(\mathbf{r}, t) = [-\frac{\nabla^2}{2} + v_{eff}(\mathbf{r}, t)] \varphi_i(\mathbf{r}, t) \quad (2.61)$$

with the initial condition

$$\varphi_i(\mathbf{r}, 0) = \varphi_i(\mathbf{r}). \quad (2.62)$$

and similar to Eq. 2.39, the time-dependent effective potential v_{eff} is

$$v_{eff}(\mathbf{r}, t) = v(\mathbf{r}, t) + v_J(\mathbf{r}, t) + v_{xc}(\mathbf{r}, t) \quad (2.63)$$

as the sum of time-dependent external potential, Coulomb interaction and exchange-correlation potential . The density of the interacting system can be obtained from the time-dependent Kohn-Sham orbitals

$$\rho(\mathbf{r}, t) = \sum_i^N f_i(t) |\varphi_i(\mathbf{r}, t)|^2 \quad (2.64)$$

where $f_i(t)$ is the time-dependent occupation number for orbital i . Therefore, if the time-dependent effective potential $v_{eff}(\mathbf{r}, t)$ can be determined, the original Schrödinger equation, a single partial differential equation in $3N$ variables, can be described by N differential equations in 3 dimensions in time dependent cases.

2.3 Solvent models

Simulating solvation is expensive if the quantum mechanical system include the solvent molecules explicitly. To model solvation effects, the conductor-like screening model (COSMO) is the chosen method to determine the electrostatic interaction of a molecule with a continuum description of the solvent. COSMO generates screening charges and forms a cavity surface within a dielectric continuum of permittivity that represents the solvent around the system [3]. Mostly the screening charges are approximately $1.2 \times$ van-der-Waals distance used as screening charge surface. COSMO uses the boundary condition of vanishing electrostatic potential for a conductor,

$$\Phi^{tot} = 0 \quad (2.65)$$

which indicates the permittivity of the ideal solvent is $\varepsilon = \infty$. The vector of the total electrostatic potential Φ^{tot} is the sum of the electrostatic potential Φ^{sol} on the cavity surface segments and the electrostatic potential Φ^{screen} generated by the screening charges q ,

$$\Phi^{tot} = \Phi^{sol} + \Phi^{screen} = 0 \quad (2.66)$$

$$\Phi^{screen} = Aq \quad (2.67)$$

$$q = -A^{-1}\Phi^{sol} \quad (2.68)$$

where A is the Coulomb matrix of the screening charge interactions. To take into account the finite permittivity of real solvents, the screening charges on the surface segments are lowered by an approximated factor [4]

$$f(\varepsilon) = \frac{\varepsilon - 1}{\varepsilon} \quad (2.69)$$

Thus, the screening charges are

$$q^* = f(\varepsilon)q. \quad (2.70)$$

2.4 Franck–Condon principle

The Franck–Condon principle explains the intensity of vibrational transitions [19]. It is the approximation that an electronic transition tends to occur with fixed positions of the nuclei, which is based on the Born–Oppenheimer approximation [6]. It states that during an electronic transition, a change from one vibrational energy level to another is proportional to the square of the overlap between the vibrational wavefunctions of the two states.

In the Born–Oppenheimer approximation, the wavefunction of a molecule to be separated into its electronic and nuclear components,

$$|\Psi_{total}(q_{nuc}, q_{el})\rangle = |\Psi_{nuc}(q_{nuc})\rangle |\Psi_{el}(q_{el}; q_{nuc})\rangle \quad (2.71)$$

Since the $\hat{\mu}$ is the dipole moment operator which depends only on the electronic component,

the probability of the transition can be written as,

$$P_{i \rightarrow f} = \langle \Psi_{total,f}^* | \hat{\mu} | \Psi_{total,i} \rangle \quad (2.72)$$

$$= \langle \Psi_{nuc,f}^* | \langle \Psi_{el,f}^* | \hat{\mu} | \Psi_{el,i} \rangle | \Psi_{nuc,i} \rangle \quad (2.73)$$

$$= \langle \Psi_{nuc,f}^* | \Psi_{nuc,i} \rangle \langle \Psi_{el,f}^* | \hat{\mu} | \Psi_{el,i} \rangle \quad (2.74)$$

The nuclear overlap part is $\langle \Psi_{nuc,f}^* | \Psi_{nuc,i} \rangle$, which means that if the integral is zero, the transition will not be observed. Thus, during the electronic transition, as the illustration in Figure 2.1, only the vertical transitions are taken into account.

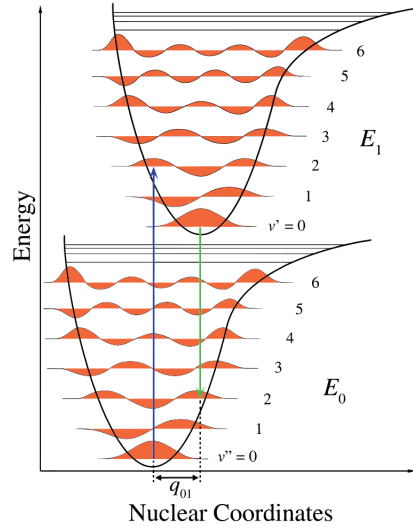


Figure 2.1: Franck Condon diagram, the figure is taken from refernce [7].

3 Computational details

3.1 Molecules in the calculations

The calculations include pyrene and its derivatives, azapyrene and diazapyrene, which show in Figure 3.1. For azapyrene (one-nitrogen substitution), the calculations include 1-azapyrene, 2-azapyrene and 4-azapyrene. For dizapyrene (two-nitrogens substitution), which has ten isomers, the calculations specifically calculate 2,7-diazapyrene, 2,10-diazapyrene.

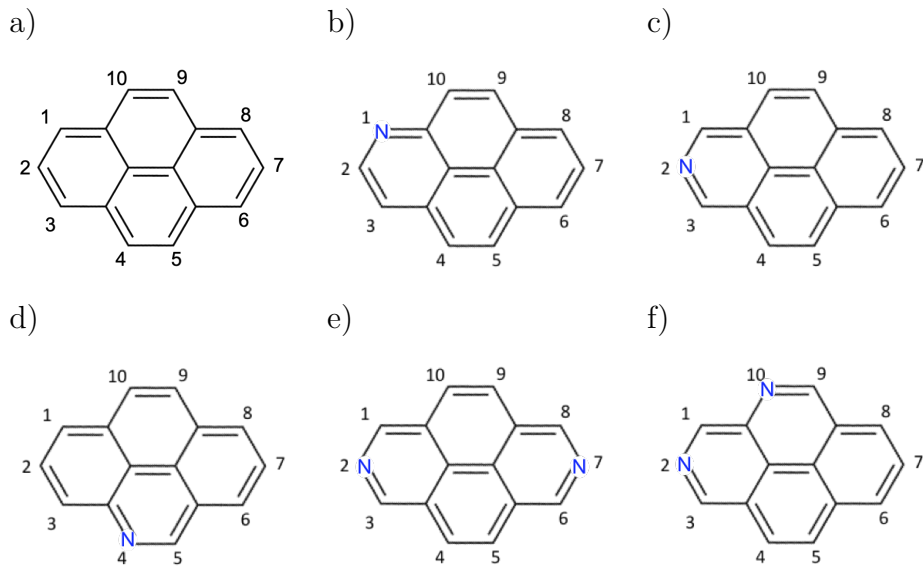
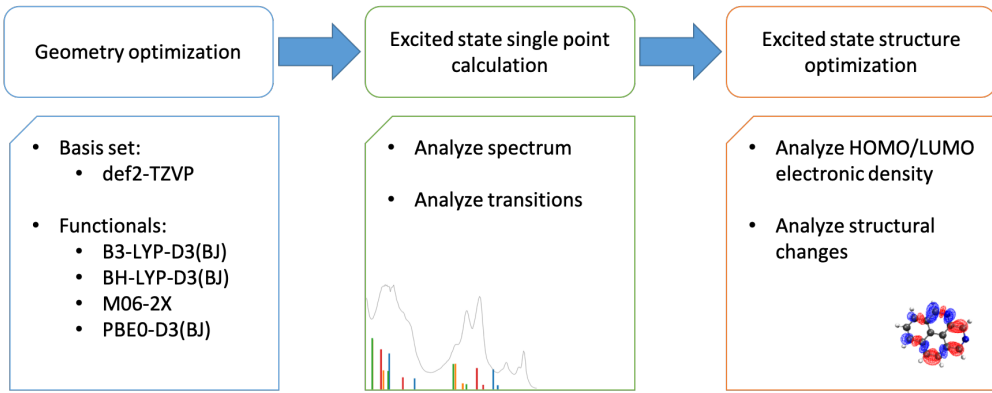


Figure 3.1: Molecules in the calculations: a) pyrene, b) 1-azapyrene, c) 2-azapyrene, d) 4-azapyrene, e) 2,7-diazapyrene, f) 2,10-diazapyrene

3.2 Calculation Procedure

The calculations are run by Turbomole 7.3, an *ab initio* computational chemistry program [24]. The procedure of calculations follow the absorbing process described in Frank-Condon diagram Figure 2.1. The geometry optimization generated the most stable state on potential surface E_0 . The excited state single point calculation generated the state on excited potential surface E_1 after vertical transition. The excited state structure optimization found the most stable state on on excited potential surface E_1 . The workflow is showed in Figure 3.2. The calculations includes DFT functionals B3-LYP-D3(BJ), BH-LYP-D3(BJ), M06-2X, and PBE0-D3(BJ).

**Figure 3.2:** Calculation workflow

3.2.1 Geometry optimization

The purpose of geometry optimization is to generate optimal (lowest energy) structures by energy minimization. During the geometry optimization in Turbomole, it iterates through self-consistent field (SCF) method, gradient and force relaxation programs until the convergence criteria (change in the total energy 10^{-8} Hartree, maximum norm of the gradient $10^{-3}a.u.$) are fulfilled or the maximum number of cycles (300) is reached. The first step of geometry run a single point calculation to obtain energy and the energy gradient. Second, the geometry updates as the quasi-Newton update:

$$q^{k+1} = q^k - F^k G^k \quad (3.1)$$

where q^k is coordinates in optimization cycle k ; F^k is the inverse of an approximate force constant matrix H^k ; G^k is the gradients from the single point calculation in first step [24]. The cycle repeats these steps until the convergence criteria mentioned above are fulfilled. The result structure is the ground state that its position on the potential energy surface (PES) is a stationary point.

3.2.2 Excited state single point calculation

Excited state single point calculations generate vertical excited states at the optimized geometries. The vertical excited state is also called Franck–Condon state, which is always a vertical transition [7]. The time-dependent DFT is utilized in excited state calculations. The calculation includes 60 singlet excitation, which can be compared with experiments using the oscillator strength representation. And it also contained the dominant contributions of orbital and energy that can determine which singlet excitation is a highest occupied molecule orbital/lowest un-occupied molecular orbital (HOMO/LUMO) excitation.

3 Computational details

3.2.3 Excited state structure optimization

With the singlet excitation that is determined in the previous step, using excited state structure optimization can find a local minimum on the excited state PES (Figure 2.1). Next, the we can analyze the structural properties and HOMO/LUMO electronic densities.

3.3 Conductor like Screening Model (COSMO)

In order to compare test molecules with solvents, acetonitrile (ACN) and dichloromethane (DCM), with experiments, COSMO, which is mentioned in Section 2.3, is included in the calculation. Approximated factors ϵ of ACN and DCM are 36.64 and 8.93, repectively.

4 Results and Discussion

This chapter presents the comparison of relative energies, different solvents and DFT functionals, calculations and experiments as well as the analysis of electronic transition of pyrene and its derivatives.

4.1 Comparison of relative energies

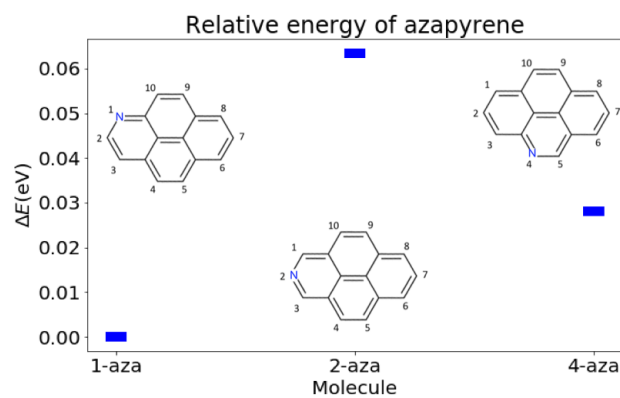


Figure 4.1: Relative energies of azapyrene derivatives at the PBE0-D3(BJ)/def2-TZVP level (Unit: eV)

In Figure 4.1 we see that 1-azaprynene is the most stable molecule with respect to other derivatives. 2-azaprynene is the least stable, in which the nitrogen substitution occurred at the symmetric position, label 2 on pyrene. The energy difference of the two is around 0.06 eV.

In Figure 4.2, among 10 isomers of diazapryrene, the 1,3-diazapryrene is the most stable molecule, the 4,5-diazapryrene is the least stable molecule with respect to other derivatives. Comparing with the difference of the most stable and least stable molecule in azapyrene derivatives, the two in diazapryrene has larger energy difference which is more than 1 eV. The results show that molecules with two neighboring nitrogen atoms are less stable, such as 4,5-diazapryrene and 1,2-diazapryrene. Take 1,2- and 1,3-diazapryrene for examples, they have common nitrogen substitution on position 1. However, their second nitrogen substitution cause a large energy difference close to 1 eV. In 1,2-diazapryrene, two nitrogens with high electrogravity are concentratedly distributed on one side of the molecule, which lead the molecule become unstable. Similarly, the 4,5 and 4,10-diazapryrene have common nitrogen

4 Results and Discussion

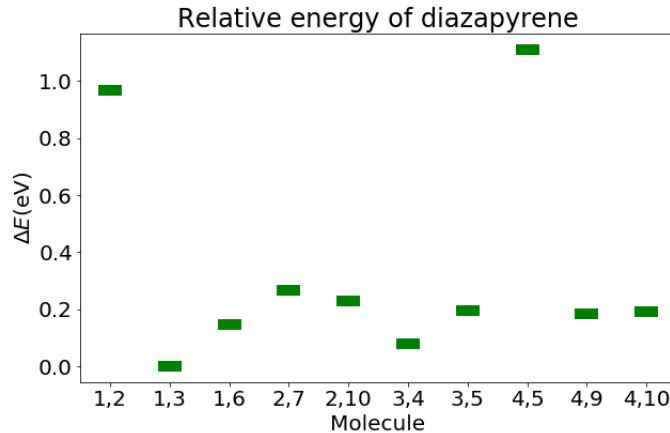


Figure 4.2: Relative energies of diazapyrene derivatives at the PBE0-D3(BJ)/def2-TZVP level (Unit: eV)

substitution on position 4. But the one with symmetrically distributed nitrogens has lower energy.

In sum, the nitrogen distribution affect the energy of molecules. If the nitrogen substitution take place at position 2, which is the symmetric part of azapyrene, the energy is higher. If two nitrogens are symmetrically distributed on diazapyrene, which “balance” to each other, the molecules are more stable.

4.2 Acetonitrile (ACN) vs. Dichloromethane (DCM) solvent

The energy difference of the highest occupied molecule orbital (HOMO) and the lowest un-occupied molecular orbital (LUMO), which is termed the HOMO/LUMO gap, is generally the lowest energy electronic excitation that is possible in a molecule. In the calculations, the Acetonitrile (ACN) and Dichloromethane (DCM) are selected as solvents in calculations. In Table 4.1, the ACN with higher ϵ has larger HOMO/LUMO gap. However, the difference of HOMO/LUMO gap is very small, it was lower than 10^{-3} eV, which shows these molecules both have a small solvent dependence. To investigate if the solvent is influential or not in our cases, the test molecules should include more azapyrene and diazapyrene derivatives.

Table 4.1: HOMO/LUMO gap using COSMO with ACN and DCM as solvents at the PBE0-D3(BJ)/def2-TZVP level (Unit: eV)

HOMO/LUMO gap	ACN ($\epsilon = 36.64$)	DCM ($\epsilon = 8.93$)	Difference (DCM - ACN)
pyrene	4.16589	4.16542	-0.00047
2,7 diazapyrene	4.05697	4.05673	-0.00024

4.3 Comparison of different DFT functionals

In Figure 4.3 and Figure 4.4, the HOMO/LUMO energy gaps of pyrene and 2,7-diazapyrene with different functionals are compared. We can observe that the LUMO energy of both are negative, which means lower excited states are still bound systems in both molecules.

The Table 4.2 indicates that the one with larger portion of Hartree-Fock exchange has larger HOMO/LUMO gap. Moreover, the results with similar portion of Hartree-Fock exchange have similar HOMO/LUMO gap in both pyrene and 2,7-diazapyrene. In both molecules, the HOMO/LUMO gap with M06-2X (54% HF exchange) are larger than BH-LYP-D3(BJ) (50% HF exchange), PBE0-D3(BJ) (25% HF exchange) and B3-LYP-D3(BJ) (20% HF exchange), in order of magnitude. Due to similar portion of Hartree-Fock exchange the PBE0-D3(BJ) and B3-LYP-D3(BJ) calculation have closer HOMO/LUMO energy gap, BH-LYP-D3(BJ) and M06-2X calculation have closer HOMO/LUMO energy gap.

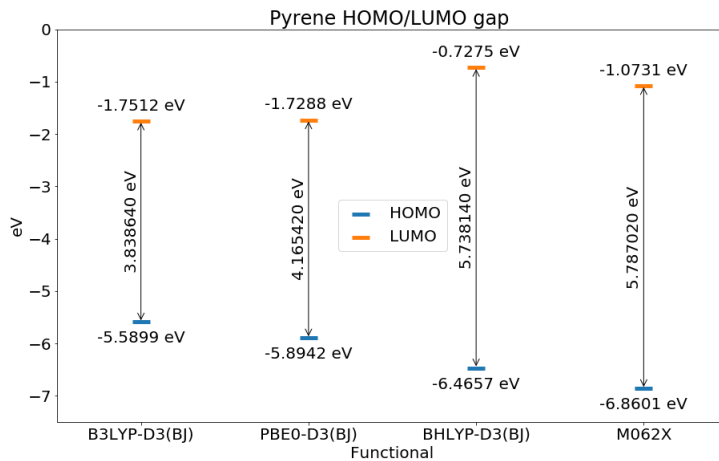


Figure 4.3: Pyrene HOMO/LUMO gap with different functionals with def2-TZVP basis set, COSMO = 36.64 (ACN), the HOMO is labeled in blue, the LUMO is labeled in orange.

Table 4.2: HOMO/LUMO gap of different functionals with def2-TZVP basis set, the difference is 2,7-diazapyrene minus pyrene energy, COSMO=36.64 (ACN) (Unit: eV).

Functional	HF exchange	Pyrene	2,7 Diazapyrene	Difference
B3-LYP	20%	3.838640	3.750190	-0.08845
PBE0	25%	4.165420	4.192700	0.02728
BH-LYP	50%	5.738140	5.793020	0.02488
M06-2X	54%	5.787020	5.825640	0.03862

4 Results and Discussion

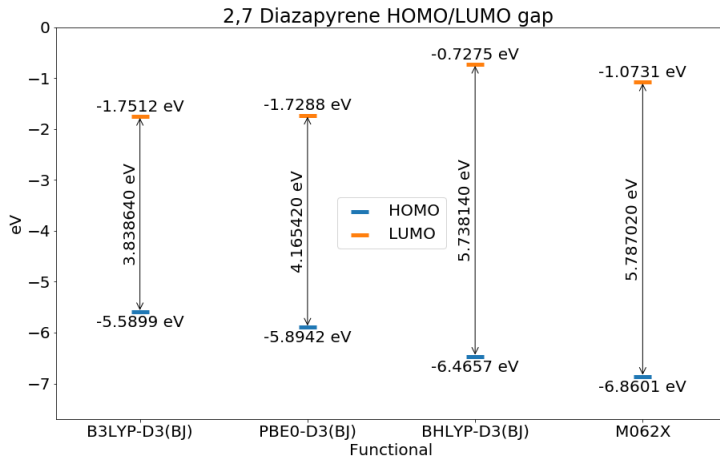


Figure 4.4: 2,7-diazapyrene HOMO/LUMO gap with different functionals with def2-TZVP basis set, COSMO = 36.64 (ACN), the HOMO is labeled in blue, the LUMO is labeled in orange.

From the aspect of nitrogen substitution, the Table 4.2 shows that the less influence of nitrogen substitution on the HOMO/LUMO energy gap, the difference between both molecule is all lower than 0.1 eV, which indicates small dependence on nitrogen substitution in excitation energies.

4.4 Comparison of calculations and experiments

The experimental spectra, DCM pyrene spectrum and ACN 2,7-diazapyrene spectrum, are provided by M.Sc. Philipp Rietsch, AG Eigler, Institut für Chemie und Biochemie, Freie Universität Berlin.

In Figure 4.5 and 4.6, as the comparison in HOMO/LUMO gap in previous section, these graph show that functional PBE0-D3(BJ) and B3-LYP-D3(BJ) have closer result, BH-LYP-D3(BJ) and M06-2X have closer result. In Figure 4.6, we can observe that the HF calculation has larger excitation energy. Moreover, the portion of HF exchange is positive correlated to the excitation energy. A possible reason is the self interaction is not exactly cancelled in the DFT. Thus, with larger portion of HF exchange, the excitation energy is larger.

The experimental patterns in Figure 4.6 and 4.5 are not perfectly match is due to the pure vertical (non-adiabatic) nature of the calculations. To get the correct patterns for the comparison, the correction of the vibrational effects is required in the Frank-Condon picture on the PES.

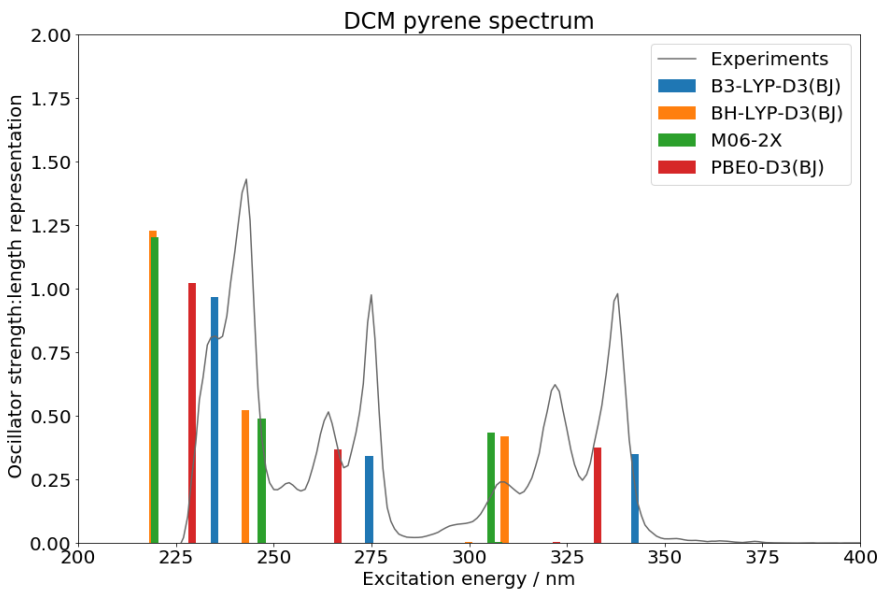


Figure 4.5: DCM pyrene spectrum

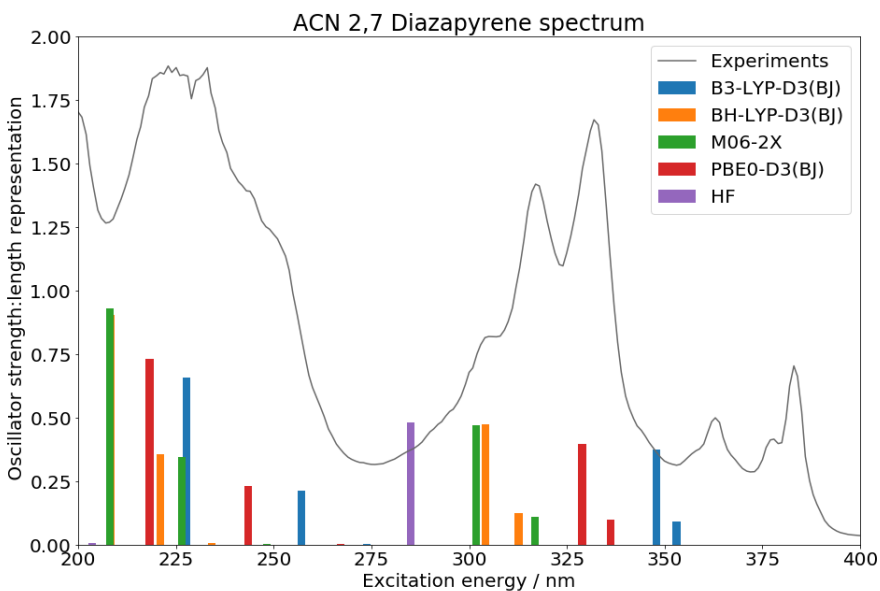


Figure 4.6: ACN 2,7-diazapyrene spectrum

4 Results and Discussion

4.5 Analysis of electronic transition

All the calculations showed in this section are calculated at the PBE0-D3(BJ)/def2-TZVP level with ACN solvent. The analysis in this section is to observe the relation between electronic transition and the bond length difference in ground state and excited state. The bond is shorter due to more electrons involved in bond formation. From Figure 4.7 to 4.12, we can observe that if the electronic density increases, the bond length become shorter from ground state to excited state, and vice versa. The HOMO/LUMO density difference $\Delta\rho$ is defined as

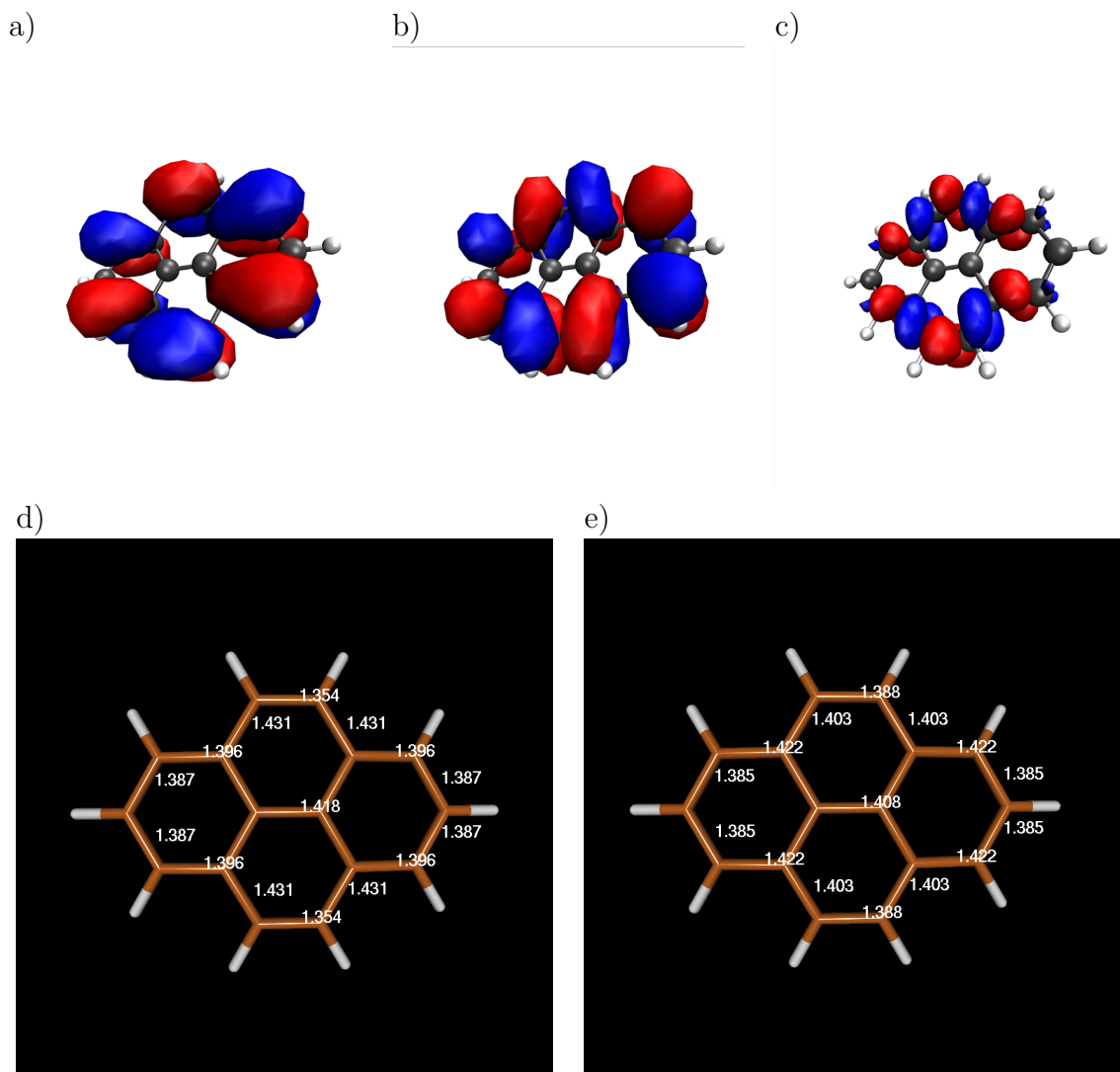
$$\Delta\rho = |\psi_{LUMO}|^2 - |\psi_{HOMO}|^2 \quad (4.1)$$

From Figure 4.7, we can observe that the nitrogen substitution on the pyrene result in the difference of electronic density between HOMO and LUMO. The atom distribution of pyrene is symmetric, thus, the electronic transition is also symmetric. Furthermore, the transition does not take place on the axis along the position 2 and position 7 (The position is illustrated in Section 3.1).

Comparing with pyrene, the HOMO/LUMO density difference of 1-azapyrene (Figure 4.8) shows that the electronic transition is different around nitrogen. The nitrogen distorts the transition with respect to the pyrene. Similarly, the nitrogen in 4-azapyrene (Figure 4.10) affects the transition. Whereas, the result of 2-azapyrene is similar as in the pyrene case. The nitrogen substitution in 2-azapyrene (Figure 4.9) is located at position 2, which is on the horizontal symmetric axis. Therefore, comparing with other isomers, the influence of nitrogen is not significant.

Similarly, because the nitrogens symmetrically distributed on 2,7-diazapyrene (position 2 and 7), these nitrogens do not have much effect on neighbor bonds. However, 2,10-diazapyrene has only one nitrogen substitution on the horizontally symmetric axis. As in previous examples, that nitrogen do not explicitly affect the electronic transition around. Another nitrogen, as in 4-azapyrene, influences more on neighbor bonding.

In sum, the bond length is negative correlated to the electronic density. Also, the position of the nitrogen affect the transition if its position is not along the horizontal axis along the position 2 and position 7. If the nitrogens lay on the horizontal axis, the parts above and below the horizontal axis can “balance” the effect of the electronegativity of nitrogens in the molecule.



4 Results and Discussion

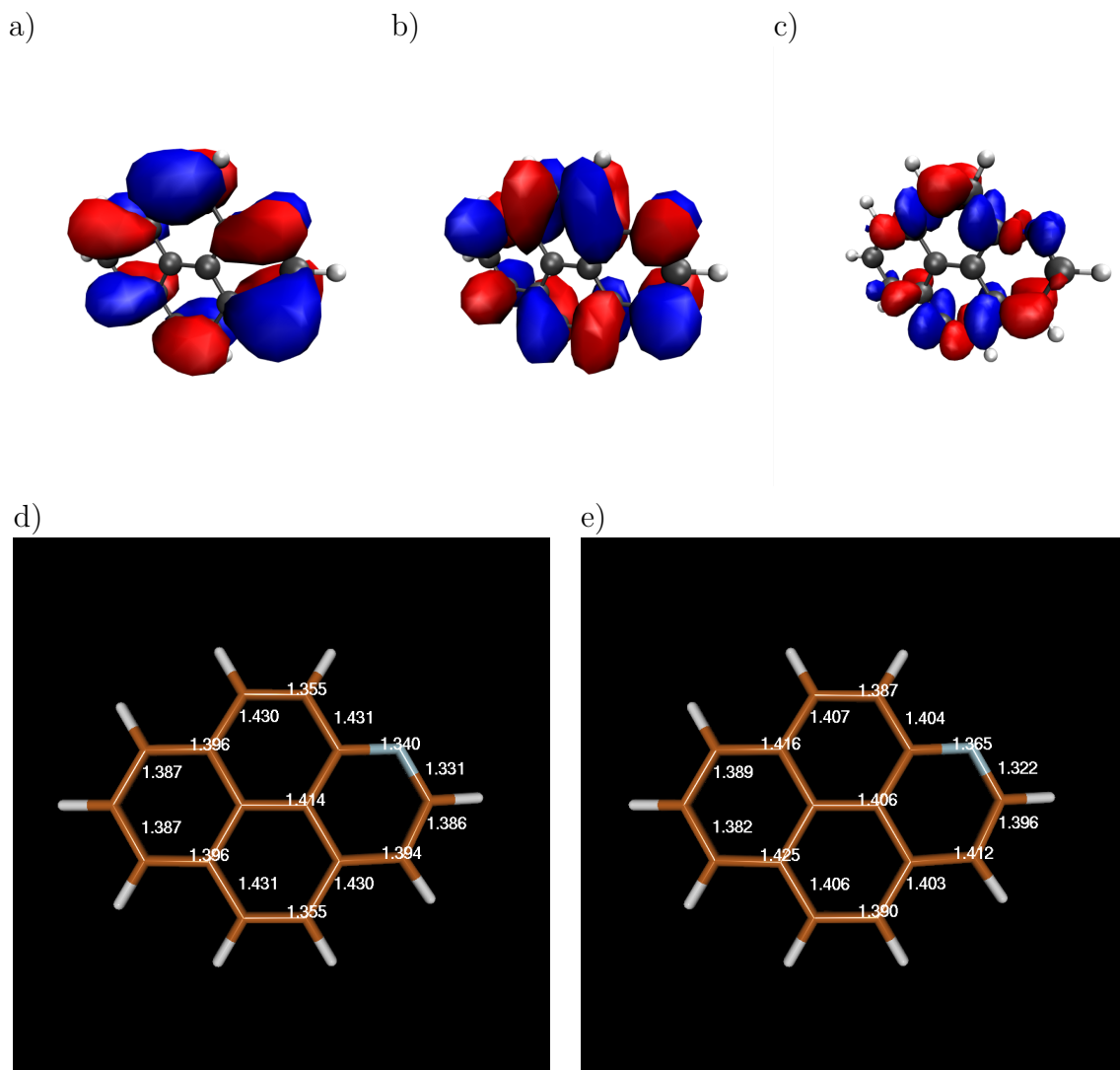


Figure 4.8: 1-azaperylene orbitals, ground and excited state bond length: a) HOMO, b) LUMO, c) $\Delta\rho$; the blue and red part represent density increased and decreased, respectively, and isovalue = $0.001 a_0^{-3}$ in a)–c). d) ground state bond lengths, e) excited state bond lengths (Unit: Å)

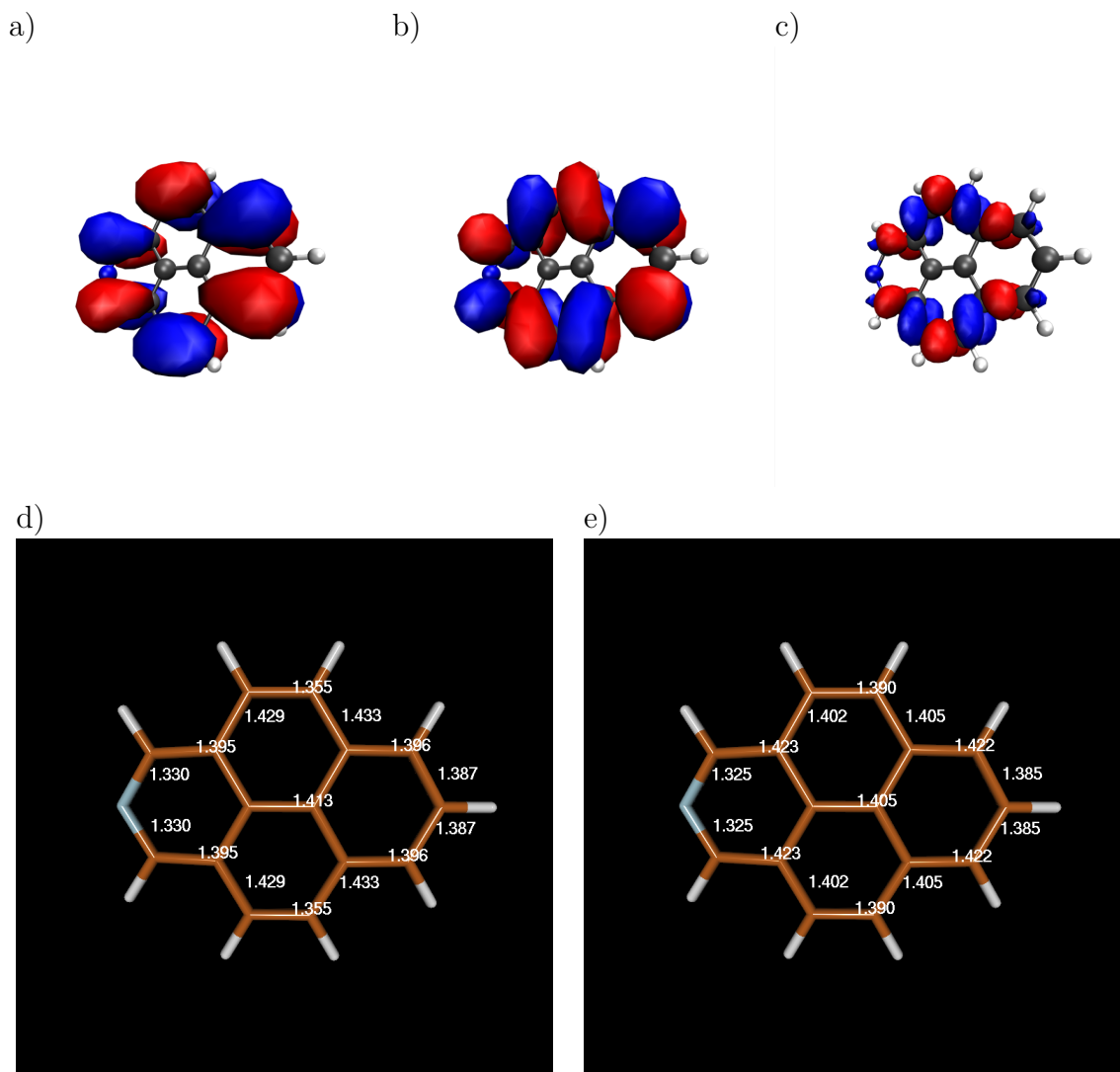
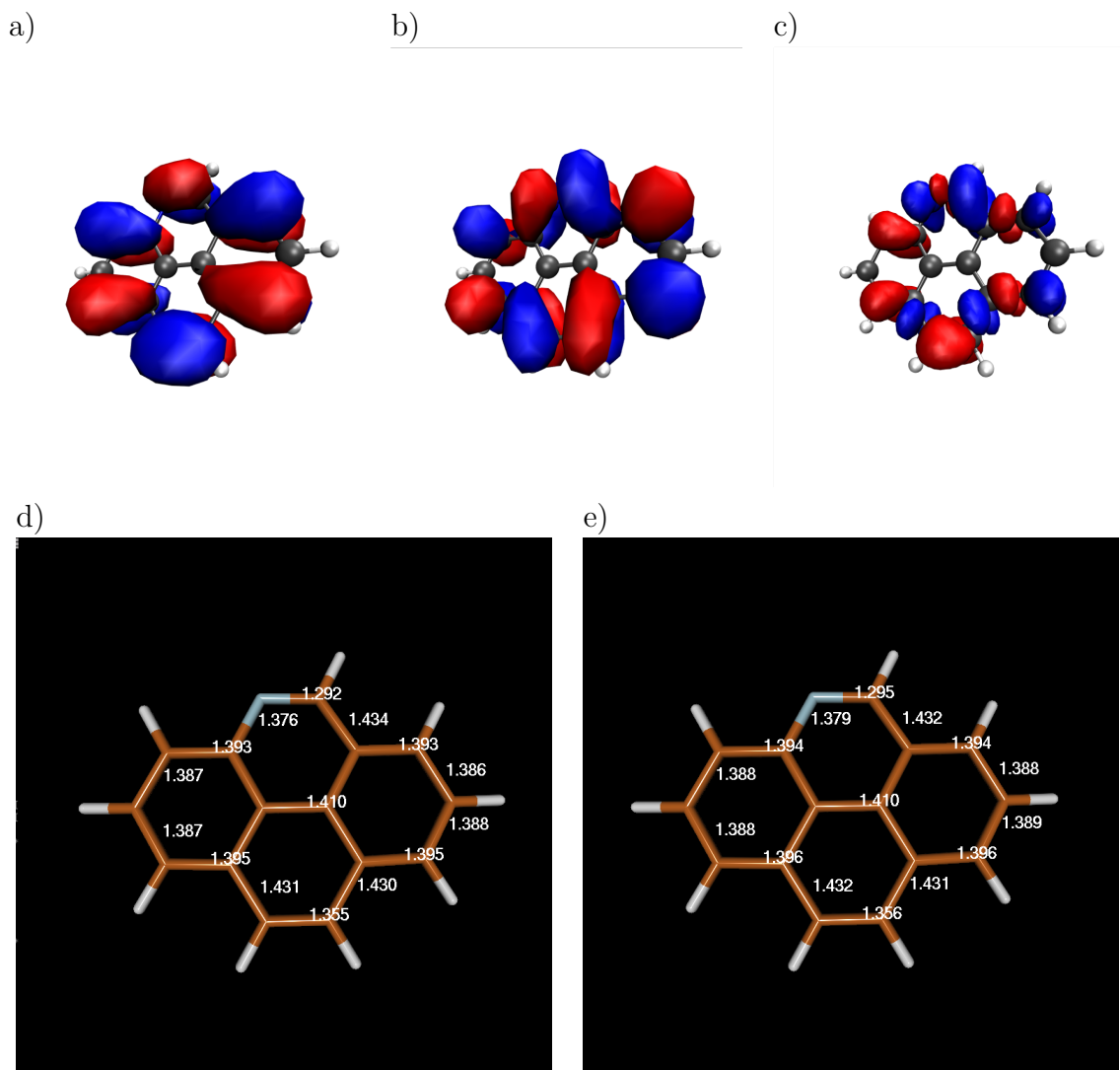


Figure 4.9: 2-azapyrene orbitals, ground and excited state bond length: a) HOMO, b) LUMO, c) $\Delta\rho$; the blue and red part represent density increased and decreased, respectively, and isovalue = $0.001 a_0^{-3}$ in a)–c). d) ground state bond lengths, e) excited state bond lengths (Unit: Å)

4 Results and Discussion



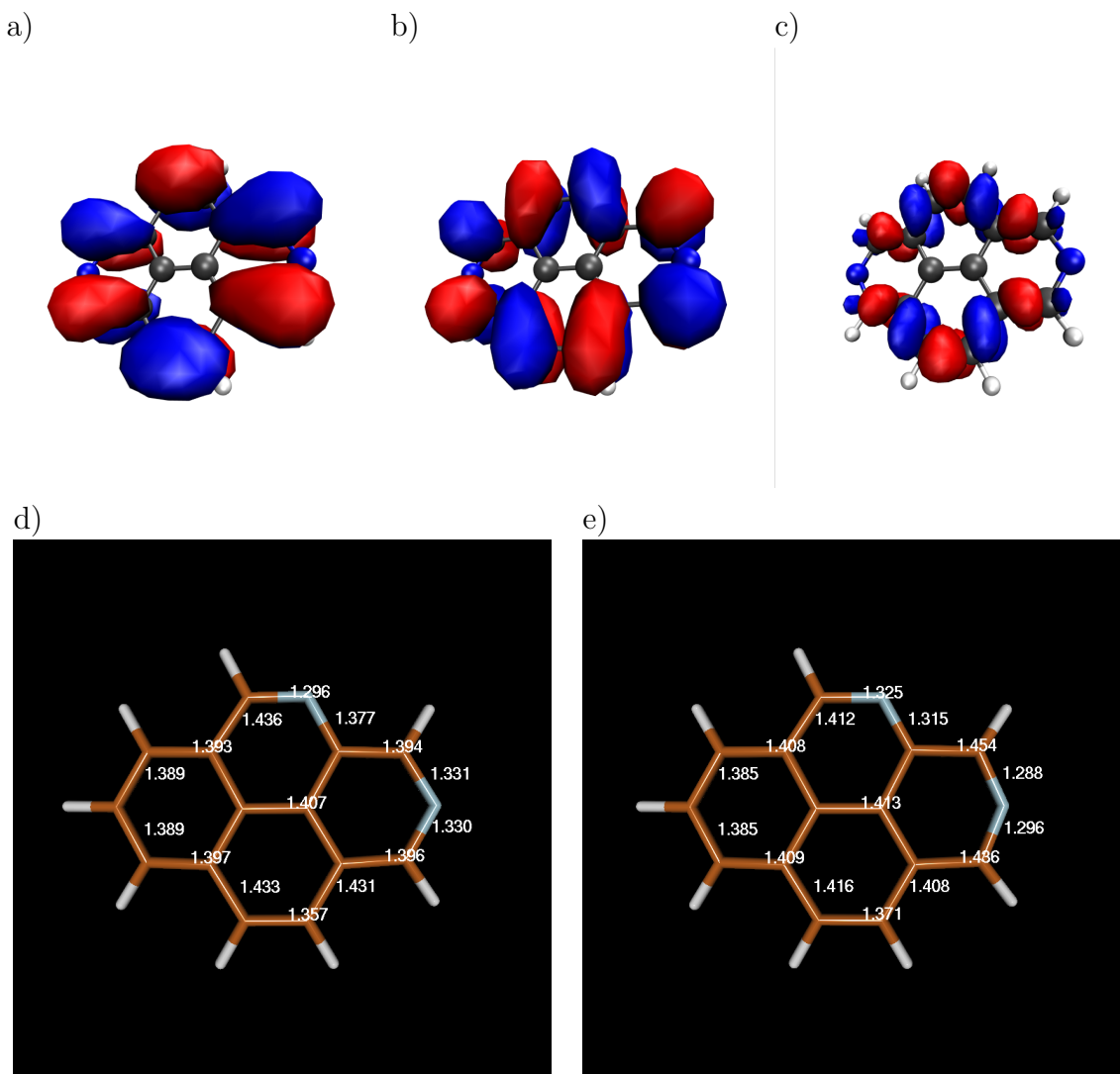


Figure 4.11: 2,7-diazapyrene orbitals, ground and excited state bond length: a) HOMO, b) LUMO, c) $\Delta\rho$; the blue and red part represent density increased and decreased, respectively, and isovalue = $0.001 a_0^{-3}$ in a)–c). d) ground state bond lengths, e) excited state bond lengths (Unit: Å)

4 Results and Discussion

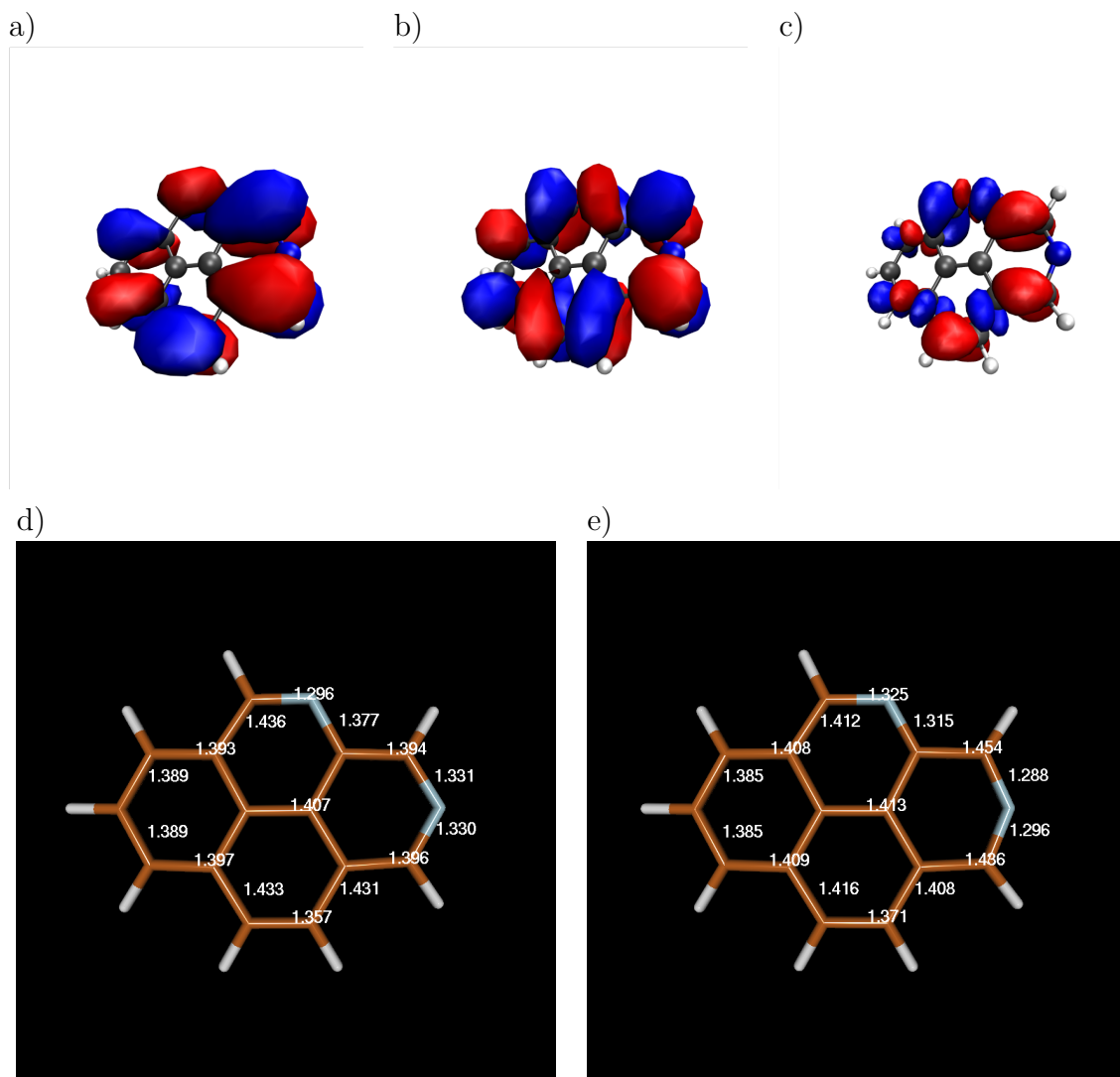


Figure 4.12: 2,10-diazapyrene orbitals, ground and excited state bond length: a) HOMO, b) LUMO, c) $\Delta\rho$; the blue and red part represent density increased and decreased, respectively, and isovalue = $0.001 \text{ } a_0^{-3}$ in a)–c). d) ground state bond lengths, e) excited state bond lengths (Unit: Å)

5 Summary and Outlook

This report studies the nitrogen substitution pattern on pyrene. The position of the nitrogen substitution results on differences in energies, and electronic structures mainly due to the large electronegativity of nitrogen. The molecules tend to be less stable if the substitutions are close, such as in 1,2-diazapyrene and 4,5-diazapyrene. Comparing the electronic structure in different molecules, we can observe that the bond length is negatively correlated to the electronic density. Moreover, the transition along with the horizontally symmetric axis is less significant even if there exist nitrogens on this axis. Furthermore, to obtain more information about the nitrogen substitution on pyrene, more calculations with its derivatives and different isomers should be involved in further calculation. Especially, since diazapyrene has ten isomers, further calculations should produce a more explicit relation between the place of substitution and the electronic transitions.

In order to investigate the dependence on solvent in the pyrene and its derivatives calculation, more molecules and solvents should be included. The current data is not enough to conclude the relation between the solvent and the HOMO/LUMO gap.

The results for different functionals (B3-LYP-D3(BJ), BH-LYP-D3(BJ), M06-2X, and PBE0-D3(BJ)) indicate the energy value, HOMO/LUMO gaps and spectrum depend on functionals. The portion of HF exchange in the functionals is positively correlated to the HOMO/LUMO energy. To observe more about the relation between calculation spectra and experiments, the correction for the vibrational effects in Frank-Condon picture is required for the experiments. Moreover, this report only contains the absorption spectra. Therefore, to obtain full information about the fluorescence, we should research in emission spectra in the future.

Bibliography

- [1] Axel D A.D. Becke. A new mixing of Hartree-Fock and local density-functional theories. *The Journal of Chemical Physics*, 98, 1993.
- [2] M.R. Roussel A.D. Becke. Exchange holes in inhomogeneous systems:A coordinate-space model. *Physical Review A*, 39(9), 1989.
- [3] A.Klamt and G. Schüürmann. COSMO:A New Approach to Dielectric Screening in Solvents with Explicit Expressions for the Screening Energy and its Gradient . *Journal of the Chemical Society*, 5, 1993.
- [4] C. Moya A.Klamt and J.Palomar. A Comprehensive Comparison of the IEFPCM and SS(V)PE Continuum Solvation Methods with the COSMO Approach. *Journal of the Chemical Theory and Computation*, 11, 2015.
- [5] Nicolas P.E. Barry and Bruno Therrien. Chapter 13 - pyrene: The guest of honor. In Samahe Sadjadi, editor, *Organic Nanoreactors*, pages 421 – 461. Academic Press, Boston, 2016.
- [6] Axel D Becke. A new mixing of Hartree-Fock and local density-functional theories. *Annalen der Physik*, 84(457), 1927.
- [7] Franck–Condon principle. Franck–condon principle — Wikipedia, the free encyclopedia, 2019.
- [8] Arti B. Patel Gursharan Bains and Vasanthy Narayanaswami. Pyrene: A Probe to Study Protein Conformation and Conformational Changes. *Molecules*, 16, 2011.
- [9] Eric J. Sorin Gursharan K. Bains, Sea H. Kim and Vasanthy Narayanaswami. Extent of Pyrene Excimer Fluorescence Emission is a Reflector of Distance and Flexibility: Analysis of the Segment Linking the LDL Receptor-binding and Tetramerization Domains of Apolipoprotein E3. *Biochemistry*, 51, 2012.
- [10] Jun Zhu JianYi Ma XiangYuan Li HaiSheng Ren, MeiJun Ming. Solvent effect on UV/Vis absorption and emission spectra in aqueous solution based on a modified form of solvent reorganization energy. *Chemical Physics Letters*, 585, 2013.

- [11] P. Hohenberg and W. Kohn. Inhomogeneous Electron Gas. *Physical Review Journals Archive*, 136, 1964.
- [12] Matthias Ernzerhof John P. Perdew and Kieron Burke. Rationale for mixing exact exchange with density functional approximations. *The Journal of Chemical Physics*, 105, 1996.
- [13] S. H. Vosko Koblar A. Jackson Mark R. Pederson D. J. Singh John P. Perdew, J. A. Chevary and Carlos Fiolhais. Atoms, molecules, solids, and surfaces: Applications of the generalized gradient approximation for exchange and correlation. *Physical Review B*, 46(6671), 1992.
- [14] K. KimK. and D. Jordan. Comparison of Density Functional and MP2 Calculations on the Water Monomer and Dimer. *The Journal of Chemical Physics*, 98, 1994.
- [15] L.D.Site. Levy-Lieb Constrained-search Formulation as Minimization of the Correlation Functional. *Journal of Physics A: Mathematical and Theoretical*, 40, 2007.
- [16] M. Levy. Electron densities in search of Hamiltonians. *Journal of Physics A: Mathematical and Theoretical*, 26, 1982.
- [17] M.A.L. Marques and E.K.U. Gross. Time-Dependent Density-Functional Theory. *Annual Review of Physical Chemistry*, 55, 2004.
- [18] Sonia E. Blanco Matias I. Sancho, Maria C. Almundoz and Eduardo A. Castro. Spectroscopic Study of Solvent Effects on the Electronic Absorption Spectra of Flavone and 7-Hydroxyflavone in Neat and Binary Solvent Mixtures. *International Journal of Molecular Sciences*, 12, 2011.
- [19] McQuarrie and Simon). *Physical Chemistry: A Molecular Approach*. 2019.
- [20] LMU München. Density functional theory, 2006.
- [21] R. G. Parr and W. Yang. *Density Functional Theory of Atoms and Molecules*. Oxford University, 1994.
- [22] Erich Runge and E. K. U. Gross. Density-Functional Theory for Time-Dependent Systems. *Physical Review Letter*, 52, 1984.
- [23] Milena I. Otradnova Tamara I. Gubina Svetlana M. Rogacheva, Elena V. Volkova and Anna B. Shipovskaya. Solvent Effect on the Solid-Surface Fluorescence of Pyrene on Cellulose Diacetate Matrices. *International Journal of Optics*, 2018, 2018.

Bibliography

- [24] Turbomole team. *Turbomole 7.3 manual*.
- [25] L. H. Thomas. The calculation of atomic fields. *Proceedings of the Cambridge Philosophical Society*, 23:542, 1927.
- [26] L. J. Sham W. Kohn. Self-Consistent Equations Including Exchange and Correlation Effects. *Journal of Physics A: Mathematical and Theoretical*, 140, 1965.
- [27] Yan Zhao and Donald G. Truhlar. Density Functional for Spectroscopy: No Long-Range Self-Interaction Error, Good Performance for Rydberg and Charge-Transfer States, and Better Performance on Average than B3LYP for Ground States. *The Journal of Chemical Physics*, 110, 2006.